ACS Sustainable Chemistry & Engineering

pubs.acs.org/journal/ascecg

Research Article

Transformation of Phosphorus during Low-Temperature Co-Combustion of Sewage Sludge with Biowastes

Xiangdong Meng, Qian Wang, Biao Wan, Jie Xu, Qunxing Huang,* Jianhua Yan, and Yuanzhi Tang*

Cite This: *ACS Sustainable Chem. Eng.* 2021, 9, 3668−3676

Read Online

ACCESS | Metrics & More | Article Recommendations | Supporting Information

ABSTRACT: Thermal treatments of phosphorus (P)-rich sewage sludge for efficient P reclamation have recently gained much attention. Our recent research proposed a low-temperature combustion method that can simultaneously target safe waste disposal, fly ash volume reduction, heavy-metal stabilization, P recovery, and energy reuse. To further optimize treatment conditions and gain deeper insights into P speciation, this study systematically characterized P transformation during low-temperature co-combustion of sewage sludge with biowaste by combining X-ray absorption spectroscopy, sequential extraction, and nuclear magnetic resonance spectroscopy analyses. Organic P, phytic acid, and pyrophosphate in the raw feedstock transformed into orthophosphate during low-temperature combustion. With increasing mass fraction of biowaste, low-temperature co-combustion increased the relative abundance of Ca-associated P and decreased the abundance of Fe-associated P. The dominant P species in the produced bottom ash is strongly correlated to the amount and speciation of metals in the feedstock and their affinities to P. The introduction of biowaste altered the enrichment efficiency and availability of P in the ash. The results from this study revealed the effects of combustion conditions and feedstock characteristics on P speciation and provided a fundamental basis for guiding the optimization of the thermal treatment method for eliminating hazardous wastes, reusing energy, and improving P reclamation efficiency.

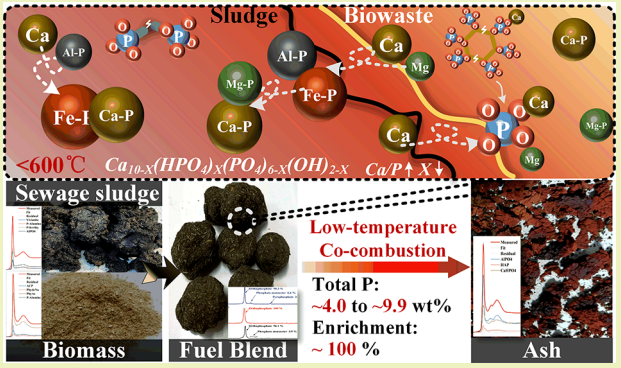

KEYWORDS: *sewage sludge, biowaste, phosphorus (P), low-temperature combustion, X-ray absorbtion spectroscopy (XAS)*

INTRODUCTION

Phosphorus (P) is an indispensable element for life and also a non-renewable resource that cannot be replaced.[1,2] It is an essential component of fertilizers for crop production.[3,4] With the increasing population, the demand for P fertilizers has increased sharply.[5] The main raw material for P-fertilizer production is the geological phosphate rock, which is estimated to be exhausted in 50−100 years at the current mining rate.[6,7] Thus, there is an urgent need to develop secondary raw materials of P to meet the increasing demand of P-fertilizer production. In this aspect, sewage sludge has been considered as a potential P resource due to the embedded high concentration of P.[8,9] However, direct application of sewage sludge to agricultural lands remains controversial since sewage sludge is also enriched with many different contaminants such as heavy metals and organic pollutants (pharmaceuticals, parasites, and pathogens),[10−13] posing potential threats to human and environmental health.

Thermal treatment of sewage sludge has many advantages such as heat energy reuse, volume reduction, and decomposition of organic pollutants.[14−16] Since a considerable amount of P is enriched in the final solids after the thermal treatment, P recovery from the treatment product is promising for the development of sewage sludge treatment technology.[17−19] However, direct incineration of sewage sludge produces a large amount of hazardous waste fly ash and reduces the concentration of P retained in bottom ash.[20] Some studies have indicated that P bioavailability of fly ash also decreased when incinerated at over 700 °C.[21−24] With this regard, our recent studies introduced a low-temperature combustion method for sewage sludge management. Compared with the disposal methods of pyrolysis and incineration, low-temperature combustion can significantly reduce the amount of fly ash and concentrate phosphorus in bottom ash, and P bioavailability in the residue could be further improved.[25]

Previous studies have reported that incineration of sewage sludge with additives such as metals or metal chlorides[26] and sodium salts can improve P bioavailability in the ash.[27] For

Received: October 28, 2020
Revised: February 9, 2021
Published: February 26, 2021

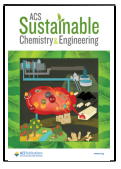

https://dx.doi.org/10.1021/acssuschemeng.0c07898
ACS Sustainable Chem. Eng. 2021, 9, 3668−3676

Table 1. Raw Materials and Masses of Low-Temperature Combustion Fuel Blends (kg)[a]

fuel blends	dewatered sewage sludge	dried corncob	dried rice hull	dried SSt	mass of dried fuel blends	ash sample label
	mass of materials before drying (kg)					
DSS	10.01 ± 0.02				2.04 ± 0.03	ash air
90% DSS/10% CP	8.99 ± 0.01	0.20 ± 0.01			1.98 ± 0.02	0.1 CP
70% DSS/30% CP	7.04 ± 0.01	0.59 ± 0.01			2.03 ± 0.02	0.3 CP
50% DSS/50% CP	5.02 ± 0.01	0.98 ± 0.01			2.01 ± 0.02	0.5 CP
50% DSS/50% RH	5.01 ± 0.02		1.00 ± 0.01		2.02 ± 0.04	0.5 RH
50% DSS/50% SSt	5.00 ± 0.01			1.01 ± 0.01	2.01 ± 0.01	0.5 SSt

[a]Notes: DSS: dried sewage sludge; CP: corncob powder; RH: rice husk; SSt: soybean straw.

Table 2. Mass Fraction of Main Chemical Constituents of DSS and Fuel Blends (wt %, as Dry Basis, Recalculated in the Oxide Form)

fuel blends	ash label	SiO_2	P_2O_5	Fe_2O_3	Al_2O_3	CaO	MgO	K_2O	Na_2O
DSS	ash air	18.0 ± 1.6	9.9 ± 0.9	9.6 ± 0.4	5.2 ± 0.2	2.8 ± 0.1	1.0 ± 0.1	0.2 ± 0.1	0.6 ± 0.1
90% DSS/10% CP	0.1 CP	16.4 ± 1.2	9.1 ± 0.8	8.6 ± 0.4	4.7 ± 0.2	2.6 ± 0.1	0.9 ± 0.1	0.4 ± 0.1	0.6 ± 0.1
70% DSS/30% CP	0.3 CP	13.9 ± 1.3	7.6 ± 0.6	6.6 ± 0.2	3.7 ± 0.1	2.2 ± 0.1	0.9 ± 0.1	0.8 ± 0.1	0.5 ± 0.1
50% DSS/50% CP	0.5 CP	9.8 ± 0.9	5.9 ± 0.5	4.8 ± 0.2	2.8 ± 0.1	1.9 ± 0.1	0.8 ± 0.1	1.1 ± 0.1	0.4 ± 0.1
50% DSS/50% RH	0.5 RH	12.7 ± 0.8	5.0 ± 0.3	4.8 ± 0.1	2.6 ± 0.1	1.8 ± 0.1	1.3 ± 0.1	0.4 ± 0.1	0.4 ± 0.1
50% DSS/50% SSt	0.5 SSt	9.1 ± 1.0	5.0 ± 0.3	4.9 ± 0.2	2.6 ± 0.2	1.9 ± 0.1	0.5 ± 0.1	0.8 ± 0.1	0.4 ± 0.1

example, the addition of $MgCl_2$, $CaCl_2$, or CaO can promote the conversion of P into new mineral phases available for plants.[28,29] Biowaste, which is rich in mineral elements (Ca, Mg, K, etc.), may also promote P transformation during thermal treatment. Studies have investigated the incineration of sewage sludge mixed with cotton stalks or wheat straw to improve the P bioavailability of fly ash.[30,31] However, few studies have investigated the speciation evolution of P during low-temperature co-combustion of sewage sludge with biowaste. The speciation (e.g., physical distribution and the chemical state) of an element is well known to affect its transport, mobility, and availability. Thus, an improved understanding of P speciation evolution during low-temperature co-combustion is necessary for optimizing P reclamation methods of sewage sludge. This study aims to systematically investigate the transformation of P during low-temperature co-combustion of sewage sludge with three common types of agricultural biowastes [corncob powder (CP), rice husk (RH), and soybean straw (SSt)] by coupling ^{31}P liquid nuclear magnetic resonance (NMR), P K-edge X-ray absorption near-edge structure (XANES), powder X-ray diffraction (XRD), and sequential extraction analyses in order to evaluate this method and reveal its fundamental knowledge basis for the development of P recycling strategies from sewage sludge.

MATERIALS AND METHODS

Materials of Sewage Sludge and Biowastes. Dewatered municipal sewage sludge was obtained from the Jiaxing Wastewater Treatment Plant, Zhejiang Province, China. Three types of agricultural biowastes, CP, RH, and SSt, were obtained from Jiangsu Province, China. Biowaste samples were dried at 105 °C in an oven over 24 h. Dried biowaste powders were passed through a 60-mesh (250 μm) sieve and then fully mixed with dewatered sewage sludge (moisture 80.0%) at different ratios (Table 1). The mixed samples were pressed into spherical pellets with a diameter of 3.0 cm and stored as fuel blends after drying at 105 °C for 24 h.

The properties of dried sewage sludge (DSS) and biowaste samples are given in Table S1, including proximate analysis (GB/T212-2001, China) and ultimate analysis (GB/T476-2001, China). The higher heating value (HHV) was measured by the ASTM D5865 standard. The main chemical constituents of the raw materials were analyzed by X-ray fluorescence (XRF, Thermo Scientific ARL 9900) and are presented in Table 2.

Co-Combustion Experiment of Fuel Blends. Co-combustion experiments were carried out in a laboratory-scale apparatus (inner diameter: 80 mm, furnace height: 300 mm), as shown in Figure S1. Five thermocouples spaced 50 mm apart are numbered 1, 2, 3, 4, and 5 from bottom to top. After the device was filled with the solid fuel, the heating plate was turned on. The bottom ash was allowed to cool down to room temperature in the furnace after combustion. The total mass of the ash and fuel was recorded. All experiments were carried out in duplicate.

Sequential Chemical Extraction. To characterize the mobility and solubility of phosphorus in sewage sludge and its thermal treatment products, the dried solids were subjected to sequential extraction following Hedley's method.[32−34] Briefly, 250 mg of the solid sample was added to a 50 mL polypropylene centrifuge tube and sequentially extracted by 20 mL extraction solutions, including deionized water (readily soluble P), 0.5 M $NaHCO_3$ (exchangeable P), 0.1 M NaOH (Fe/Al mineral adsorbed P), and 1.0 M HCl (insoluble phosphates) solution, each lasting 16 h by end-to-end shaking. The residual fraction and total P were measured after digestion using aqua regia at 100 °C. The aqueous phases and solids were separated by filtration (0.45 μm) at the end of each step. The P bioavailability of the ash samples was analyzed by using neutral ammonium citrate (NAC) and 2% citric acid (CA) according to EU regulation no. 2003/2003 (EU. 2003).[35,36] The P concentration in the solutions was determined with the molybdenum blue method using a UV−vis spectrometer (Carey 60, Agilent).[37]

P K-Edge XANES Analysis. Phosphorus K-edge XANES spectroscopy allows non-invasive direct identification of P species in complex matrixes. P K-edge XANES data were obtained at Beamline 14−3 at the Stanford Synchrotron Radiation Lightsource (SSRL), Menlo Park, CA, USA. Powdered P reference standards and samples (e.g., sewage sludge, biowaste, and ashes) were spread homogeneously onto a Kapton film. The sample compartment was maintained under a He atmosphere. The energy was calibrated by setting the edge position (maximum energy of the first peak in the first derivative) for $AlPO_4$ to 2152.8 eV. The spectra were recorded in the fluorescence mode using a PIPS detector at photon energies between 2100 and 2485 eV. Multiple spectra were recorded for each sample and averaged for further analysis.

As shown in Table 2, Al, Ca, Fe, and Mg are the main cations which may form metal phosphate salts or P complexation in fuel blends and ashes. Therefore, spectra of their corresponding P compounds were selected as references for linear combination fitting

https://dx.doi.org/10.1021/acssuschemeng.0c07898
ACS Sustainable Chem. Eng. 2021, 9, 3668−3676

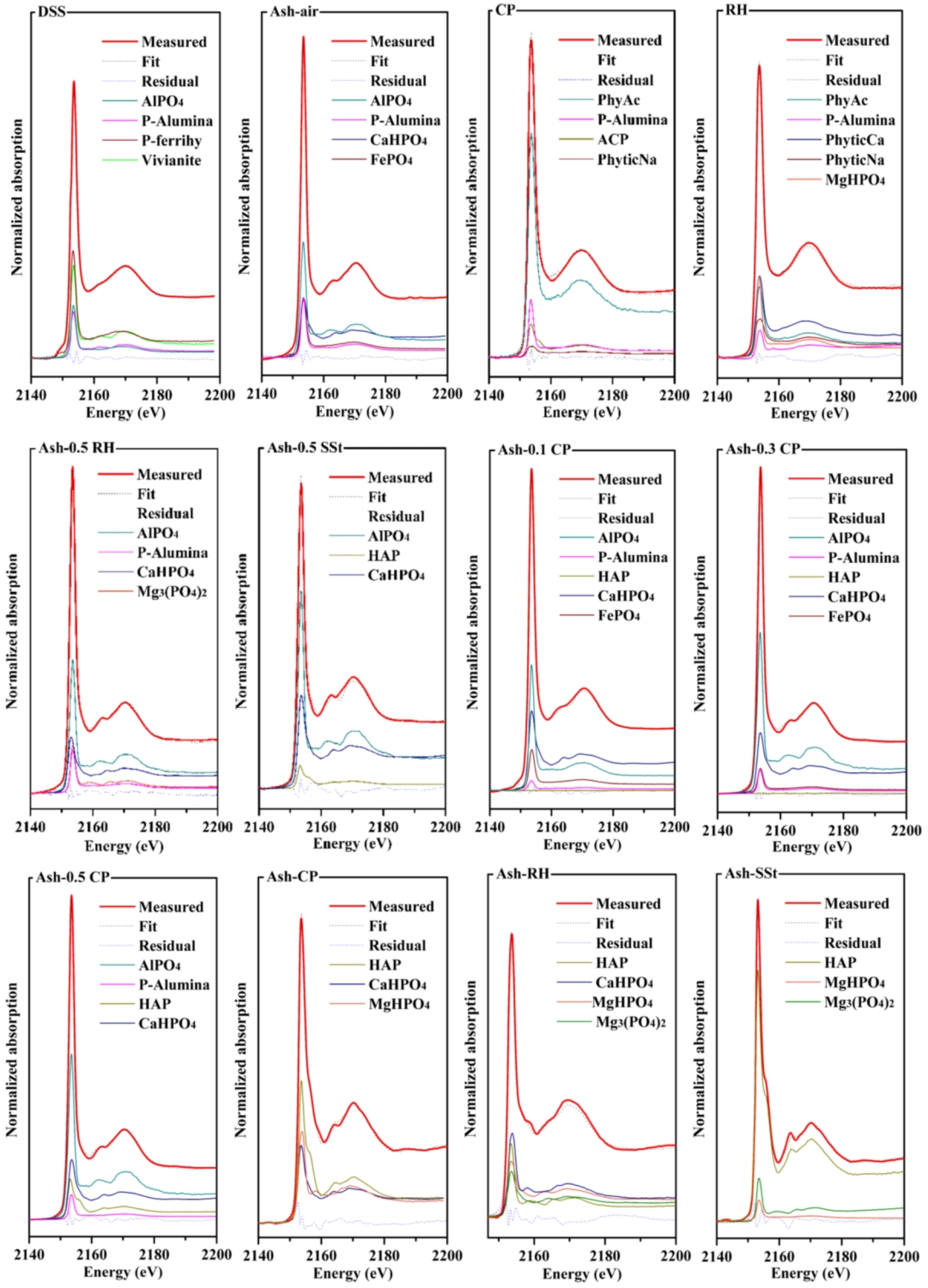

Figure 1. Linear combination fitting of P XANES spectra of DSS, biowastes, bioashes, and co-combustion ashes. Fitting results are shown in Figure 2 and Table S3.

(LCF), including Al-associated P (phosphate sorbed on γ-alumina and $AlPO_4$), Ca-associated P ($CaHPO_4$, amorphous Ca phosphorus, and hydroxyapatite), Fe-associated P (vivianite, ferrihydrited-adsorbed P, and $FePO_4$), Mg-associated P [$Mg_3(PO_4)$ and $MgHPO_4$], and organic P (phytic acid, Na phytate, and Ca phytate). Details of all reference compounds are present in Table S2 and Figure S2.

Data processing used the software SIXPack and ATHENA. All XANES spectra were examined for energy calibration and merged. LCF was performed at an energy range of −15 to +50 eV relative to the edge energy E_0. The goodness of fit was evaluated using the residual factor (R factor), and the fit with the smallest R factor was deemed the best fit.

Powder X-ray Diffraction Analysis. Powder XRD (Philps X'pert PRO) was used to detect the main crystalline compounds in the ash samples. The instrument was equipped with Cu Kα radiation, and the data were obtained in the range of 10−80° with a scan step of 0.02°.

https://dx.doi.org/10.1021/acssuschemeng.0c07898
ACS Sustainable Chem. Eng. 2021, 9, 3668−3676

Liquid ^{31}P Nuclear Magnetic Resonance Spectroscopy. Sewage sludge and its thermal-treated products were extracted using a solution containing 0.25 M NaOH and 0.05 M ethylenediaminetetraacetic acid at a solid/liquid ratio of 0.2:4 g/mL and were shaken at 150 rpm for 16 h at room temperature. The solid and aqueous phases were separated by centrifugation. The extracted solution was mixed with D_2O (100 μL) for measurements. ^{31}P NMR spectra of liquid samples were recorded using a Bruker AMX 400 MHz spectrometer operated at 162 MHz at 297 K. A 90° pulse width, 6.5 K data points (TD) over an acquisition time of 0.51 s, and a relaxation delay of 15 s were applied.

RESULTS AND DISCUSSION

Chemical Characterization of Sewage Sludge, Biowaste, and Fuel Blends. As shown in Table S1, the volatiles and HHV of the three biowastes (66−74%, >15000 KJ·kg^{-1}) are much higher than those of DSS (46%, about 6400 KJ·kg^{-1}), while the ash content of biowastes (<12.0 wt %) is less than that of DSS (48 wt %). Increasing the biowaste mass fraction reduces the ash content and increases the volatile and HHV of fuel blends. During the combustion process, the high volatility and HHV of fuel blends are beneficial for its ignition and self-sustained combustion in the insulating furnace. The low ash content can effectively reduce heat loss and increase the contact area between air and the solid fuel, which benefits its sufficient combustion. Therefore, the introduction of biowaste contributes to the efficient, stable, and sufficient combustion of sludge-based fuels.

XRF results in Table 2 indicate that Si, Fe, Al, and P are the major elements of DSS and fuel blends. Overall, DSS has a higher P content (P_2O_5 at ∼9.9%) than fuel blends (4.8−8.7%). The contents of Al and Fe decreased by ∼50% when biowastes were mixed with sludge at a 1:1 ratio. This is because the higher contents of organic compounds and volatility lead to relatively low P, Al, and Fe contents in biowaste. It is worth noting that the concentrations of Ca, Mg, and K did not decrease significantly in fuel blends. For example, the Ca content decreased by ∼30% (compared to a 40−50% decrease for P) for fuel blends mixed with 50 wt % of biowaste, which suggests that the ratio of Ca/P in fuel blends (a molar ratio at 0.36−0.48) was higher than that in DSS (∼0.35). As for magnesium, the addition of RH increased its content in fuel blends to over 30%. It indicates that the contents of Ca, Mg, and K in the three biowastes are relatively high as compared to sewage sludge. Specifically, the concentrations of Ca in corncob and SSt are high, and the Mg content in RH is the most abundant among the three biowastes. Overall, the introduction of biowaste increased the ratio of the metal (Ca or Mg, depends on the species of biowaste) to P.

P XANES spectra of DSS and the biowastes showed significant difference in P speciation (Figures 1 and 2, Table S3). Ferrihydrite-adsorbed phosphate (37%), $AlPO_4$ (34%), vivianite (17%), and alumina-adsorbed phosphate (12%) are the four dominant species identified in DSS. The dominant P species in biowastes is organic P. Phytate (78% for phytic acid and Na/Ca-phytate), amorphous Ca phosphate (11%), and alumina-adsorbed phosphate (11%) are the main P species in CP, while phytate (71%), $MgHPO_4$ (16%), and alumina-adsorbed phosphate (14%) are identified in RH. Moreover, P moieties in the liquid extracts of raw and combusted sewage sludge were detected by ^{31}P liquid NMR. Figure 3 shows the dominant presence of orthophosphate (90%) and small fractions of pyrophosphate (7%) and phosphate monoester (3%) for the liquid extract of raw sludge. Orthophosphate

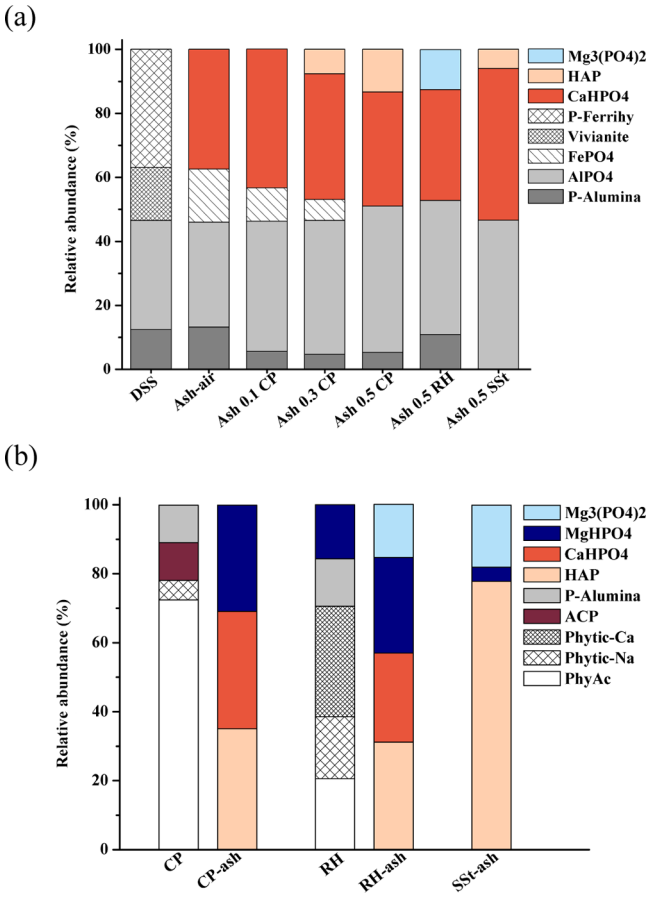

Figure 2. Relative abundance of different P species in DSS and co-combustion ashes (a) corncob, RH, SSt, and their ash (b), as quantified by LCF of their P XANSE spectra.

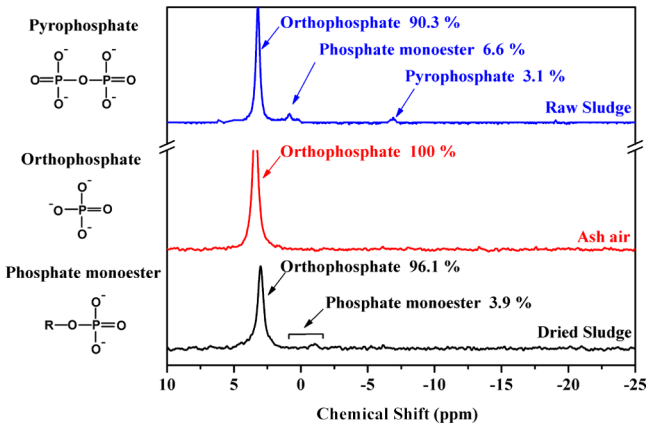

Figure 3. ^{31}P NMR spectra of the liquid extracts of dewatered sludge, dried sludge, and the derived combustion ash.

(96%) and phosphate monoester (4%) were identified in the liquid extract of DSS.

P species in DSS are mostly Fe/Al-associated P in the form of orthophosphate; no Ca-associated P or organic P was detected. The presence of abundant Ca phytate, amorphous Ca phosphate, and $MgHPO_4$ in corncob and RH is consistent with the element composition results showing abundant Ca and Mg. Due to the low concentration of P in SSt, we were not able to obtain good fitting on its P XANES spectrum. Since

https://dx.doi.org/10.1021/acssuschemeng.0c07898
ACS Sustainable Chem. Eng. 2021, 9, 3668−3676

phytate is ubiquitous in plant straw, it is reasonable to expect organic P as the dominate P species in SSt.

Characteristics and P Enrichment Efficiency of the Co-Combustion Products. Figure S3 shows the co-combustion temperature profile of DSS and fuel blends. The four curves (numbers 1−4) in each figure are the temperatures measured using the four thermocouples with the same numbers in Figure S1. The reaction was self-sustained (without an external heating source after ignition) at relatively low temperatures (below 600 °C). The temperature recorded by the no. 5 thermocouple is not shown in Figure S3. This is because the fuel blends in the insulating furnace gradually sank during the combustion process, causing the no. 5 thermocouple to be out of contact with the reaction zone.

As shown in Figure S3, the spread rate of the combustion front and the highest combustion temperature of DSS were 0.027 mm/s and 565.1 °C, respectively. The spread rate increased to 0.066, 0.049, and 0.056 mm/s with the mixing of RH, corncob, and SSt, respectively. The peak temperature during the co-combustion of sewage sludge with CP reached 604.9 °C, which was the highest among the three biowastes. The other two biowastes had no significant effects on the peak temperature of combustion (both were lower than 600 °C). The combustion method used in this study can increase the combustion rate of fuel blends and maintain the combustion temperature below around 600 °C. Under these conditions, the organic pollutants in sludge can be degraded, while P volatilization caused by high temperatures (>800 °C) was inhibited, which improved the P enrichment efficiency and led to a high P-concentration solid product (bottom ash).[25,38]

The volatilization of organic P and mechanical carryover may lead to transformation of P into fly ash, which is not conducive to P enrichment in bottom ash. To further investigate the effect of low-temperature co-combustion with biowastes on P enrichment efficiency, we compared the P recovery efficiency of the ash from low-temperature co-combustion with those of different biowaste additives. Similar to the definition of heavy-metal retention by Li et al.,[39] the P enrichment efficiency E of the ash can be defined as

$$E = \frac{P_{ash} \times M_{ash}}{P_{fuel} \times M_{fuel}} \times 100\% \quad (1)$$

where P_{fuel} and P_{ash} are the P contents (mg/g) in dried fuel blends and co-combusted ashes, respectively, and M_{fuel} and M_{ash} are the masses of fuel blends and co-combusted ashes, respectively. E_{ash} is the mass recovery of ash from low-temperature co-combustion of sewage sludge with biowaste and is defined as

$$E_{ash} = \frac{M_{ash}}{M_{fuel}} \times 100\% \quad (2)$$

Table S4 shows the content of phosphorus and the enrichment rate of total P in the ash. The ash recovery efficiency of DSS is 47%, which is slightly higher than its ash content (46%), as shown in Table S1. This difference may be caused by the incomplete combustion of fixed carbon in DSS. As the corncob mass fraction in fuel blends increased from 10 to 50%, E_{ash} decreased from 44 to 26%. The addition of RH and SSt also led to a decrease in the ash recovery efficiency. The P enrichment efficiency of DSS is about 90%, while it is 95, 98, and 100% for the samples 0.1 CP, 0.3 CP, and 0.5 CP, respectively. These results suggest that the P enrichment efficiency of fuel blends increases with increasing corncob mass fraction. When RH was used as the additive, the P enrichment efficiency of the sample 0.5 RH is about 86%, which was slightly lower than that of DSS. SSt has no obvious effect on the P enrichment efficiency, which is about 90%. As shown in Table 2, the contents of P_2O_5, CaO, and K_2O of the fuel blend with 50 wt % CP are higher than those of the other two fuel blends. The reaction between P and alkali metals such as K and Ca in biowastes during the combustion leads to the formation of stable K−Ca−P compounds with a high melting temperature, which is beneficial for reducing the volatilization of P and the formation of particulate matter, thereby increasing the P enrichment efficiency in the bottom ash.[30,40] Thus, CP is more effective on the enrichment of phosphorus in ash than RH and SSt.

P Speciation Change during Low-Temperature Co-Combustion. As shown in Figure 1, P XANES spectra of all the ash samples showed increasing degrees of the distinctive feature of Ca-associated P (peaks at ∼2164 and ∼2172 eV), the presence of which was confirmed by LCF analysis. Specifically, after the low-temperature combustion of DSS, the decrease of Fe-associated P (17% vivianite and 37% P-Ferrihy for DSS, 17% $FePO_4$ for the ash) and the formation of Ca-associated P were the dominant changes based on P XANES LCF analysis (Figures 1 and 2, Table S3). The relative abundance of Al-associated P ($AlPO_4$ and alumina-adsorbed phosphate) remains at around 46% for both DSS and its derived ash. Compared to the high abundance of organic P in the raw biowastes, organic P was not identified in their derived ashes. Mg- and Ca-associated P (including $CaHPO_4$ and hydroxyapatite) increased in the biowaste-derived ashes as compared to the raw biowastes. When 50 wt % biowaste (CP, RH, or SSt) was used in the fuel blends, no Fe-associated P was identified in the corresponding ash products. The relative abundance of Fe- and Ca-associated P in the corncob-mixed fuel blend ashes shows an inverse correlation with the mass fraction of corncob. For example, 17% $FePO_4$ in DSS ash gradually decreased to 10, 7%, and 0 for 0.1 CP, 0.3 CP and 0.5 CP, respectively. The relative abundance of Ca-associated P increased from ∼37% for DSS ash to 43, 47, and 49% for 0.1 CP, 0.3 CP, and 0.5 CP, respectively, which suggests stronger association of P with Ca due to the introduction of CP in the fuel blends. Meanwhile, 7.6% hydroxyapatite (HAP) was identified in the ash of 0.3 CP, which further increased to 13.3% for 0.5 CP. Interestingly, instead of HAP, 12.5% $Mg_3(PO_4)_2$ was identified in the ash of 0.5 RH, which was likely caused by the high Mg content in raw RH.

P Speciation Probed by Sequential Chemical Extraction. Hedley's sequential extraction method is extensively used to empirically determine the mobility and speciation of P in solid matrixes. Here, we use this method to characterize P speciation in the sewage sludge and its thermal-treated products to complement P XANES results. Sequential extraction results (Figure 4 and Table S5) showed that P in DSS and its derived ash has low mobility, with the total relative abundance of H_2O and $NaHCO_3$ extractable fractions at about 5%. The NaOH and HCl fractions of DSS are at 60 and 27%, respectively. After low-temperature combustion, the NaOH fraction decreased from 60% for DSS to 49% for DSS ash, and the HCl fraction increased from 27 to 36%, respectively. For ashes derived from the combustion of fuel blends, the enhancement was more significant for the HCl fraction, which generally increased with increasing biowaste mass

https://dx.doi.org/10.1021/acssuschemeng.0c07898
ACS Sustainable Chem. Eng. 2021, 9, 3668−3676

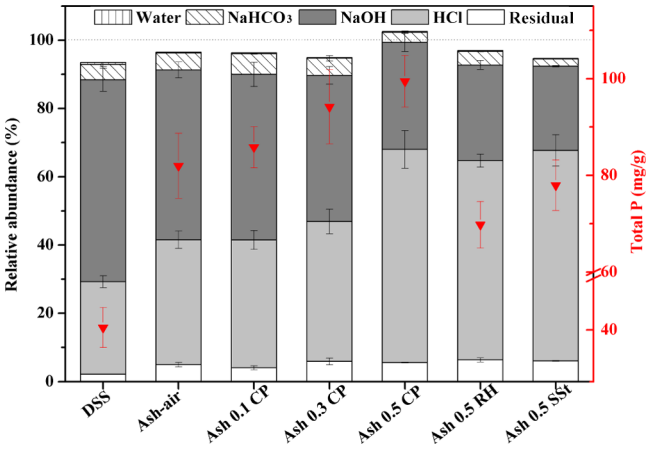

Figure 4. Total content and distribution of P in sequential extracts of sewage sludge and its co-combustion ash.

fraction. For example, the HCl fraction of 0.5 CP was at 62% as compared to 37 and 40% for 0.1 CP and 0.3 CP, respectively. Meanwhile, the NaOH fraction decreased to 30% for 0.5 CP as compared to 48 and 43% for 0.1 CP and 0.3 CP, respectively. The introduction of RH and SSt also showed similar enhancement in HCl and NaOH fractions in the co-combusted ashes. Specifically, the HCl fraction increased to 58% (for 0.5 RH) and 62% (for 0.5 SSt) and the NaOH fraction decreased to 28% (for 0.5 RH) and 25% (for 0.5 SSt), as compared to 49% (HCl fraction) and 36% (NaOH fraction) for DSS ash.

The stabilization of P in sewage sludge by combustion has been observed in previous studies.[28,41,42] To further reveal the stabilization mechanism of P, the results from LCF analysis of P XANES were compared to those from the sequential chemical extraction. Some research studies indicated that ferrihydrite-adsorbed P and Al-adsorbed P are readily extracted during the NaOH step and Ca-associated P cannot react during the H_2O−$NaHCO_3$−NaOH steps.[18,43] In this study, the relative abundance of vivianite (17% in DSS) and ferrihydrite-adsorbed P (37% in DSS) decreased and the NaOH fraction significantly decreased in the DSS-derived ash. Ca-associated P formed ($CaHPO_4$ 37%) and contributed to the increase of the HCl fraction in the DSS-derived ash. In comparison, the relative abundance of Al-associated P (P-alumina and $AlPO_4$) remained relatively stable in DSS and all ashes. This suggests that a portion of vivianite and ferrihydrited-adsorbed P converted to $FePO_4$ and Ca-associated P during the combustion of DSS. The NaOH fraction continued to decrease from 49% for DSS-derived ash to 30% for 0.5 CP, consistent with the observed decrease of the $FePO_4$ fraction detected by LCF analysis of P XANES. Such trends on the change of Fe-associated fractions were enhanced with the increase of biowaste mass fraction. For example, when 50 wt % of biowastes (CP, RH, or SSt) was used in fuel blends, no Fe-associated P was detected, and the NaOH fraction was mostly contributed from $AlPO_4$.

P Transformation Mechanism and Its Effect on Bioavailability. As discussed above, P speciation has transformed through different pathways during low-temperature co-combustion of sewage sludge with biowaste. In the case of P molecular configurations, low-temperature co-combustion transformed organic P (e.g., phytic acid and Na/Ca-phytate) and pyrophosphate into orthophosphate, which subsequently reacted with metal cations to form P-containing minerals, surface-adsorbed phases, or P-metal cation complexes. The chemical states of P in the combustion products depend on the type and abundance of metal cation species (e.g., Al, Ca, Fe, and Mg) in the feedstock. The relative abundance of $AlPO_4$, $FePO_4$, and $CaHPO_4$ increased in the ash derived from the co-combustion as compared to DSS. On the other hand, the affinity of P to the metal cation (i.e., Fe, Al, Ca, and Mg) is different depending on the metal cation type. Some studies indicated that Al and Fe phosphate minerals can transform to Ca-phosphate phases during incineration of sewage sludge.[44−46]

In this study, the increasing abundance of Ca in the CP, SSt, and RH blended fuels increased the contact and reaction probability of Ca with $FePO_4$, $AlPO_4$, or orthophosphate released from organic P degradation. Figure S4 shows the main P-containing mineral phases in the DSS and ashes detected by XRD. $AlPO_4$ and $FePO_4$ are the dominant P species in DSS and its ashes. For all three biowastes, when the biowaste mass fraction reached 50%, Fe-associated P completely disappeared with the appearance of Ca-associated P after co-combustion. The intensity of diffraction peaks for $Ca_{18}Mg_2H_2(PO_4)_{14}$ is enhanced in the sample 0.5 RH, which is consistent with P XANES LCF results showing the formation of Mg-associated phosphate in the ash as the addition of RH provided more Mg source. In addition, P immobilization was enhanced after co-combustion with the increase of Ca-phosphate mineral crystallinity, such as the formation of crystalline $Ca_2P_2O_7$, $Ca(PO_3)_2$, $CaHPO_4$, and hydroxyapatite $[Ca_{10}(PO_4)_6(OH)_2]$, as shown in Figure S4. $CaHPO_4$ can be decomposed at >450 °C and converted into crystalline $Ca_2P_2O_7$. Meanwhile, the reaction of $AlPO_4$ and $FePO_4$ with Ca compounds can form $Ca_2P_2O_7$ and $Ca(PO_3)_2$.[44] With increasing mass fraction of CP, the abundance of hydroxyapatite gradually increased and the relative abundance of $CaHPO_4$ decreased. The molar ratio of Ca/P gradually increased from 0.35 for DSS to 0.36 and 0.41 for fuel blends with 30 wt % and 50 wt % CP, respectively. The increasing ratio of Ca/P in the blended feedstock (all below 1.67) likely contributed more Ca source for the transformation of calcium-deficient apatite [CDHA, $Ca_{10-x}(HPO_4)_x(PO_4)_{6-x}(OH)_{2-x}$] into HAP (which begins to lose water at 850 °C but is stable at temperatures below 1200 °C[47]). The transformation from CDHA to HAP possibly led to the increase of HAP relative abundance and the decrease of $CaHPO_4$ based on LCF of P XANES. Chlorapatite $[Ca_5(PO_4)Cl]$ and $Ca_9HPO_4(PO_4)_5OH$ were identified in the 0.5 CP sample by XRD, which confirmed the formation of CDHA during combustion. Meanwhile, the high content of chlorine in biowaste likely induced the formation of the Ca−P−Cl mineral.[48,49] Overall, the increasing abundance of the Ca-phosphate mineral and HAP formation from different pathways enhanced P immobilization with increasing biowaste fraction.

We further conducted solubility tests to evaluate the availability of the P species in the co-combustion ash. Figure S5 shows the P solubility of the DSS and ash samples in NAC and 2% CA, which was a previously used indicator for evaluating P availability for plants.[50] P solubility in the CA test is positively correlated with the amount of Ca-associated P phases.[16] Chien (1993) showed that the solubility of Fe- and Al-associated P is much greater than that of apatite P using the NAC solubility test;[51] thus, P solubility in NAC can be used to indicate the relative abundance of Fe/Al-associated P minerals as compared to Ca-associated P minerals,[35,51] with Fe/Al-

https://dx.doi.org/10.1021/acssuschemeng.0c07898
ACS Sustainable Chem. Eng. 2021, 9, 3668−3676

associated P minerals typically having lower availability than Ca-associated P minerals.

Using the NAC and CA tests, we observed an increase of P solubility in CA from 47 to 65 mg/g with increasing CP mass fraction from 0 to 30%, corresponding to 57% and 65% of total P, respectively. When the CP mass fraction increased to 50% (the sample 0.5 CP), P solubility in CA further increased to 79 mg/g, reaching 75% of total P in this sample. As previously discussed, the relative abundance of Ca-associated P in the samples 0.5 CP and 0.5 SSt was relatively high, and P solubility in CA accounted for more than 70% of the total P for both samples. Meanwhile, solubilized P in NAC gradually decreased from 40 mg/g for the sample DSS to 30 mg/g for 0.5 CP. The sample 0.5 SSt has the lowest P solubility of 19 mg/g in NAC. The relatively low P solubility in NAC of co-combusted ashes as compared to the sample DSS ash, in combination with the increase of CA-soluble P in co-combusted ashes, confirmed that co-combustion with biowastes improved the transformation of Fe- and Al-phosphate into Ca-associated P. Thus, the low-temperature co-combustion with biowaste, especially with the addition of Ca-rich CP, enhanced P availability in the final ash products.

CONCLUSIONS

This study systematically characterized the P transformation during low-temperature co-combustion of sewage sludge with different biowastes at varied mixing ratios, revealed the transformation mechanism of P speciation from both the molecular moiety and mineralogy aspects, and explored the effects of combustion and feedstock characteristics on the P species and bioavailability in the ash products. In general, the introduction of biowaste contributed to the efficient, stable, and sufficient combustion of the sludge-biowaste blends. Organic P and pyrophosphate in the fuel blends transformed into orthophosphate during combustion. The released orthophosphate reacted with metal cations to form P-containing phases, and the affinity of phosphate to Ca was stronger than that of Fe and Al. The relative abundance and transformation pathways of different P species were dependent on the fuel blend composition such as the type and concentration of dominant metal cations. $FePO_4$ was fully converted to Ca/Mg-associated phosphate minerals with increasing mass fraction of biowaste in the fuel blends, which contributed to more Ca/Mg source.

A better understanding of the transformation mechanism of P speciation provides insights into the design of disposal techniques and treatment conditions for sewage sludge and other biowastes to achieve efficient P recovery and recycling. For example, more attention needs to be paid to the type and concentration of dominant metal cations (e.g., Al, Ca, Mg, and Fe) in biowastes and sewage sludge while introducing high-volatile and HHV biowastes to optimize low-temperature combustion of sewage sludge. High Ca-concentration biowastes used for blending can lead to more Ca-associated P in ash products, which has a significant contribution to P availability. In summary, the results from this study provide the fundamental basis for low-temperature co-combustion of organic solid waste such as sewage sludge and biowaste as well as a guidance for the optimization of thermal treatment techniques with higher efficiency of energy reuse and P reclamation.

ASSOCIATED CONTENT

Supporting Information

The Supporting Information is available free of charge at https://pubs.acs.org/doi/10.1021/acssuschemeng.0c07898.

Proximate and ultimate analysis of solid samples, reference compounds used for XANES LCF analyses, XANES LCF analysis results of samples, P enrichment rate of ashes, experimental apparatus, normalized P XANES spectra of reference compounds, combustion temperature curves, XRD patterns of ash samples, and P solubility in CA and NAC of ashes (PDF)

AUTHOR INFORMATION

Corresponding Authors

Qunxing Huang − *State Key Laboratory of Clean Energy Utilization, Institute for Thermal Power Engineering of Zhejiang University, Hangzhou 310027, China;* orcid.org/0000-0003-1557-3955; Phone: +86-571-87952834; Email: hqx@zju.edu.cn

Yuanzhi Tang − *School of Earth and Atmospheric Sciences, Georgia Institute of Technology, Atlanta, Georgia 30332-0340, United States;* orcid.org/0000-0002-7741-8646; Phone: +1-404-894-3814; Email: yuanzhi.tang@eas.gatech.edu

Authors

Xiangdong Meng − *State Key Laboratory of Clean Energy Utilization, Institute for Thermal Power Engineering of Zhejiang University, Hangzhou 310027, China; School of Earth and Atmospheric Sciences, Georgia Institute of Technology, Atlanta, Georgia 30332-0340, United States*

Qian Wang − *School of Earth and Atmospheric Sciences, Georgia Institute of Technology, Atlanta, Georgia 30332-0340, United States*

Biao Wan − *School of Earth and Atmospheric Sciences, Georgia Institute of Technology, Atlanta, Georgia 30332-0340, United States*

Jie Xu − *State Key Laboratory of Clean Energy Utilization, Institute for Thermal Power Engineering of Zhejiang University, Hangzhou 310027, China*

Jianhua Yan − *State Key Laboratory of Clean Energy Utilization, Institute for Thermal Power Engineering of Zhejiang University, Hangzhou 310027, China*

Complete contact information is available at: https://pubs.acs.org/10.1021/acssuschemeng.0c07898

Notes

The authors declare no competing financial interest.

ACKNOWLEDGMENTS

This work received the support of the National Key Research and Development Program of China (2018YFC1901300), the National Natural Science Foundation of China (grant no. 51621005), the U.S. National Science Foundation (grant no. 1739884), the Key Research and Development Program of Yunnan Science and Technology Department (2018IB026), the China Scholarship Council, and the Zhejiang University Scholarship for Outstanding Doctoral Candidates. We appreciate Dr. Rixiang Huang, Dr. Matthias Egge, Dr. Florian Werner, and Dr. Christian Vogel for sharing their XANES spectra of P reference compounds. We thank beamline scientists at BL 14-3 at the SSRL for technical assistance

https://dx.doi.org/10.1021/acssuschemeng.0c07898
ACS Sustainable Chem. Eng. 2021, 9, 3668−3676

data collection. A portion of this research was conducted at SSRL, a U.S. Department of Energy (DOE) Office of Science User Facility operated for the DOE Office of Science by SLAC National Accelerator Laboratory under contract no. DE-AC02-76SF00515.

REFERENCES

(1) Desmidt, E.; Ghyselbrecht, K.; Zhang, Y.; Pinoy, L.; Van der Bruggen, B.; Verstraete, W.; Rabaey, K.; Meesschaert, B. Global Phosphorus Scarcity and Full-Scale P-Recovery Techniques: A Review. *Crit. Rev. Environ. Sci. Technol.* **2015**, *45*, 336−384.
(2) Liu, Y.; Qu, H. Design and optimization of a reactive crystallization process for high purity phosphorus recovery from sewage sludge ash. *J. Environ. Chem. Eng.* **2016**, *4*, 2155−2162.
(3) Liu, y.; Villalba, G.; Ayres, R. U.; Schroder, H. Global Phosphorus Flows and Environmental Impacts from a Consumption Perspective. *J. Ind. Ecol.* **2008**, *12*, 229−247.
(4) Neset, T.-S. S.; Cordell, D. Global Phosphorus Scarcity: Identifying Synergies for a Sustainable Future. *J. Sci. Food Agric.* **2012**, *92*, 2−6.
(5) Chowdhury, R. B.; Moore, G. A.; Weatherley, A. J.; Arora, M. A review of recent substance flow analyses of phosphorus to identify priority management areas at different geographical scales. *Resour. Conserv. Recycl.* **2014**, *83*, 213−228.
(6) Li, R.; Yin, J.; Wang, W.; Li, Y.; Zhang, Z. Transformation of phosphorus during drying and roasting of sewage sludge. *Waste Manag.* **2014**, *34*, 1211−1216.
(7) Shepherd, J. G.; Kleemann, R.; Bahri-Esfahani, J.; Hudek, L.; Suriyagoda, L.; Vandamme, E.; Van Dijk, K. C. The future of phosphorus in our hands. *Nutrient Cycl. Agroecosyst.* **2016**, *104*, 281−287.
(8) Cieślik, B.; Konieczka, P. A review of phosphorus recovery methods at various steps of wastewater treatment and sewage sludge management. The concept of "no solid waste generation" and analytical methods. *J. Clean. Prod.* **2017**, *142*, 1728−1740.
(9) Havukainen, J.; Nguyen, M. T.; Hermann, L.; Horttanainen, M.; Mikkilä, M.; Deviatkin, I.; Linnanen, L. Potential of phosphorus recovery from sewage sludge and manure ash by thermochemical treatment. *Waste Manag.* **2016**, *49*, 221−229.
(10) Donatello, S.; Cheeseman, C. R. Recycling and recovery routes for incinerated sewage sludge ash (ISSA): A review. *Waste Manag.* **2013**, *33*, 2328−2340.
(11) Donatello, S.; Tong, D.; Cheeseman, C. R. Production of technical grade phosphoric acid from incinerator sewage sludge ash (ISSA). *Waste Manag.* **2010**, *30*, 1634−1642.
(12) Herzel, H.; Krüger, O.; Hermann, L.; Adam, C. Sewage sludge ash—A promising secondary phosphorus source for fertilizer production. *Sci. Total Environ.* **2016**, *542*, 1136−1143.
(13) Tarayre, C.; De Clercq, L.; Charlier, R.; Michels, E.; Meers, E.; Camargo-Valero, M.; Delvigne, F. New perspectives for the design of sustainable bioprocesses for phosphorus recovery from waste. *Bioresour. Technol.* **2016**, *206*, 264−274.
(14) Saleh Bairq, Z. A.; Li, R.; Li, Y.; Gao, H.; Sema, T.; Teng, W.; Kumar, S.; Liang, Z. New advancement perspectives of chloride additives on enhanced heavy metals removal and phosphorus fixation during thermal processing of sewage sludge. *J. Clean. Prod.* **2018**, *188*, 185−194.
(15) Carbonell, G.; Pro, J.; Gómez, N.; Babín, M. M.; Fernández, C.; Alonso, E.; Tarazona, J. V. Sewage sludge applied to agricultural soil: Ecotoxicological effects on representative soil organisms. *Ecotoxicol. Environ. Saf.* **2009**, *72*, 1309−1319.
(16) Wang, T.; Camps-Arbestain, M.; Hedley, M.; Bishop, P. Predicting phosphorus bioavailability from high-ash biochars. *Plant Soil* **2012**, *357*, 173−187.
(17) Hossain, M. K.; Strezov, V.; Chan, K. Y.; Ziolkowski, A.; Nelson, P. F. Influence of pyrolysis temperature on production and nutrient properties of wastewater sludge biochar. *J. Environ. Manage.* **2011**, *92*, 223−228.
(18) Huang, R.; Tang, Y. Speciation Dynamics of Phosphorus during (Hydro)Thermal Treatments of Sewage Sludge. *Environ. Sci. Technol.* **2015**, *49*, 14466−14474.
(19) Yao, J.; Li, W.-B.; Kong, Q.-N.; Wu, Y.-Y.; He, R.; Shen, D.-S. Content, mobility and transfer behavior of heavy metals in MSWI bottom ash in Zhejiang province, China. *Fuel* **2010**, *89*, 616−622.
(20) Lin, Y.-C.; Yen, J.-H.; Lateef, S. K.; Hong, P.-K. A.; Lin, C.-F. Characteristics of residual organics in municipal solid waste incinerator bottom ash. *J. Hazard. Mater.* **2010**, *182*, 337−345.
(21) Ottosen, L. M.; Kirkelund, G. M.; Jensen, P. E. Extracting phosphorous from incinerated sewage sludge ash rich in iron or aluminum. *Chemosphere* **2013**, *91*, 963−969.
(22) Guedes, P.; Couto, N.; Ottosen, L. M.; Ribeiro, A. B. Phosphorus recovery from sewage sludge ash through an electrodialytic process. *Waste Manag.* **2014**, *34*, 886−892.
(23) Yuan, Z.; Pratt, S.; Batstone, D. J. Phosphorus recovery from wastewater through microbial processes. *Curr. Opin. Biotechnol.* **2012**, *23*, 878−883.
(24) Beck, J.; Unterberger, S. The behaviour of phosphorus in the flue gas during the combustion of high-phosphate fuels. *Fuel* **2006**, *85*, 1541−1549.
(25) Meng, X.; Huang, Q.; Gao, H.; Tay, K.; Yan, J. Improved utilization of phosphorous from sewage sludge (as Fertilizer) after treatment by Low-Temperature combustion. *Waste Manag.* **2018**, *80*, 349−358.
(26) Fraissler, G.; Jöller, M.; Mattenberger, H.; Brunner, T.; Obernberger, I. Thermodynamic equilibrium calculations concerning the removal of heavy metals from sewage sludge ash by chlorination. *Chem. Eng. Process: Process Intensif.* **2009**, *48*, 152−164.
(27) Stemann, J.; Peplinski, B.; Adam, C. Thermochemical treatment of sewage sludge ash with sodium salt additives for phosphorus fertilizer production—Analysis of underlying chemical reactions. *Waste Manag.* **2015**, *45*, 385−390.
(28) Adam, C.; Peplinski, B.; Michaelis, M.; Kley, G.; Simon, F.-G. Thermochemical treatment of sewage sludge ashes for phosphorus recovery. *Waste Manag.* **2009**, *29*, 1122−1128.
(29) Han, J.; Kanchanapiya, P.; Sakano, T.; Mikuni, T.; Furuuchi, M.; Wang, G. The behaviour of phosphorus and heavy metals in sewage sludge ashes. *Int. J. Environ. Pollut.* **2009**, *37*, 357−368.
(30) Ren, Q.; Li, L. Co-combustion of Agricultural Straw with Municipal Sewage Sludge in a Fluidized Bed: Role of Phosphorus in Potassium Behavior. *Energy Fuels* **2015**, *29*, 4321−4327.
(31) Zhao, Y.; Ren, Q.; Na, Y. Influence of operating parameters on arsenic transformation during municipal sewage sludge incineration with cotton stalk. *Chemosphere* **2018**, *193*, 951−957.
(32) Hedley, M. J.; Stewart, J. W. B.; Chauhan, B. S. Changes in Inorganic and Organic Soil Phosphorus Fractions Induced by Cultivation Practices and by Laboratory Incubations. *Soil Sci. Soc. Am. J.* **1982**, *46*, 970−976.
(33) Wang, Q.; Zhang, C.; Liu, P.; Jung, H.; Wan, B.; Patel, D.; Pavlostathis, S. G.; Tang, Y. Effect of interstage hydrothermal treatment on anaerobic digestion of sewage sludge: speciation evolution of phosphorus, iron, and sulfur. *ACS Sustainable Chem. Eng.* **2020**, *8*, 16515−16525.
(34) Wang, Q.; Zhang, C.; Patel, D.; Jung, H.; Liu, P.; Wan, B.; Pavlostathis, S. G.; Tang, Y. Coevolution of iron, phosphorus, and sulfur speciation during anaerobic digestion with hydrothermal pretreatment of sewage sludge. *Environ. Sci. Technol.* **2020**, *54*, 8362−8372.
(35) Steckenmesser, D.; Vogel, C.; Adam, C.; Steffens, D. Effect of various types of thermochemical processing of sewage sludges on phosphorus speciation, solubility, and fertilization performance. *Waste Manag.* **2017**, *62*, 194−203.
(36) Zhao, Y.; Ren, Q.; Na, Y. Promotion of cotton stalk on bioavailability of phosphorus in municipal sewage sludge incineration ash. *Fuel* **2018**, *214*, 351−355.
(37) Öhlinger, R. Soil Sampling and Sample Preparation. *Methods in Soil Biology*; Springer, 1996; pp 7−11.

https://dx.doi.org/10.1021/acssuschemeng.0c07898
ACS Sustainable Chem. Eng. 2021, 9, 3668−3676

(38) Thygesen, A. M.; Wernberg, O.; Skou, E.; Sommer, S. G. Effect of incineration temperature on phosphorus availability in bio-ash from manure. *Environ. Technol.* **2011**, *32*, 633−638.
(39) Li, R.; Teng, W.; Li, Y.; Wang, W.; Yang, T.; Zhang, Z. Coenrichment characteristics of phosphorus and heavy metals in incinerated sewage sludge ash. *Environ. Prog. Sustain. Energy* **2016**, *35*, 1027−1034.
(40) Zhu, Y.; Fan, J.; Yang, P.; Cheng, W.; Zeng, K.; Zhang, W.; Yang, H.; Shao, J.; Wang, X.; Chen, H. P-based additive for reducing fine particulate matter emissions during agricultural biomass combustion. *Energy Fuels* **2019**, *33*, 11274−11284.
(41) Peplinski, B.; Adam, C.; Michaelis, M.; Kley, G.; Emmerling, F.; Simon, F.-G. Reaction sequences in the thermochemical treatment of sewage sludge ashes revealed by X-ray powder diffraction—A contribution to the European project SUSAN. *Z. Kristallogr.* **2009**, *2009*, 459−464.
(42) Qian, T.-T.; Jiang, H. Migration of Phosphorus in Sewage Sludge during Different Thermal Treatment Processes. *ACS Sustainable Chem. Eng.* **2014**, *2*, 1411−1419.
(43) Kar, G.; Hundal, L. S.; Schoenau, J. J.; Peak, D. Direct chemical speciation of P in sequential chemical extraction residues using P K-edge X-ray absorption near-edge structure spectroscopy. *Soil Sci.* **2011**, *176*, 589−595.
(44) Li, R.; Zhang, Z.; Li, Y.; Teng, W.; Wang, W.; Yang, T. Transformation of apatite phosphorus and non-apatite inorganic phosphorus during incineration of sewage sludge. *Chemosphere* **2015**, *141*, 57−61.
(45) Yang, F.; Chen, J.; Yang, M.; Wang, X.; Sun, Y.; Xu, Y.; Qian, G. Phosphorus recovery from sewage sludge via incineration with chlorine-based additives. *Waste Manag.* **2019**, *95*, 644−651.
(46) Li, R.; Teng, W.; Li, Y.; Wang, W.; Cui, R.; Yang, T. Potential recovery of phosphorus during the fluidized bed incineration of sewage sludge. *J. Clean. Prod.* **2017**, *140*, 964−970.
(47) Trombe, J. C.; Montel, G. Some features of the incorporation of oxygen in different oxidation states in the apatitic lattice-I On the existence of calcium and strontium oxyapatites. *J. Inorg. Nucl. Chem.* **1978**, *40*, 15−21.
(48) Johansen, J. M.; Jakobsen, J. G.; Frandsen, F. J.; Glarborg, P. Release of K, Cl, and S during pyrolysis and combustion of high-chlorine biomass. *Energy Fuels* **2011**, *25*, 4961−4971.
(49) Miles, T. R.; Miles, T. R., Jr; Baxter, L. L.; Bryers, R. W.; Jenkins, B. M.; Oden, L. L. Boiler deposits from firing biomass fuels. *Biomass Bioenergy* **1996**, *10*, 125−138.
(50) Vogel, C.; Adam, C.; Peplinski, B.; Wellendorf, S. Chemical reactions during the preparation of P and NPK fertilizers from thermochemically treated sewage sludge ashes. *Soil Sci. Plant Nutr.* **2010**, *56*, 627−635.
(51) Chien, S. H. Solubility assessment for fertilizer containing phosphate rock. *Fert. Res.* **1993**, *35*, 93−99.

https://dx.doi.org/10.1021/acssuschemeng.0c07898
ACS Sustainable Chem. Eng. 2021, 9, 3668−3676